PHYSICAL REVIEW B VOLUME 49, NUMBER 2 1 JANUARY 1994-II

Random-phase-approximation analysis of orbital- and magnetic-fluctuation-mediated superconductivity in a two-band Hubbard model

F. Buda* and D. L. Cox
Department of Physics, The Ohio State University, 174 West 18th Avenue, Columbus, Ohio 43210

M. Jarrell
Department of Physics, University of Cincinnati, Cincinnati, Ohio 45221-0011

(Received 17 June 1993)

We have applied a generalized random phase approximation analysis to a two-band Hubbard model for the cuprate superconductors which treats magnetic and orbital (quadrupolar) fluctuations on an equal footing and which allows for significant itinerant character of the copper d electrons. The two bands represent the lowest copper orbitals. We qualitatively reproduce the known results of antiferromagnetic order at half filling with an adjoining region of d-wave-symmetry superconductivity in the single-band limit. When the value of the band splitting is comparable to the hopping integral of the x^2-y^2 orbitals, we find a qualitatively new region of superconductivity at increased hole doping which is clearly associated with orbital (quadrupolar) fluctuations and a significant $x^2-y^2 \rightarrow 3z^2-r^2$ charge transfer but no concommitant charge or magnetic order. The pairs are very spread out in momentum and energy space. At the optimal temperature for the new instability, the Fermi surface has two sheets, and d-wave and s-wave pair states are nearly degenerate. We discuss the possible phenomenological relevance of these results to photoemission and other data for the cuprates.

I. INTRODUCTION

The high-temperature cuprate superconductors present a fundamental challenge to our understanding of strongly correlated materials. By this point it is all but certain that the mechanism for the superconductivity is novel in the sense of being electronically based. However, it appears likely that the superconducting states themselves may be of a rather conventional "s-wave" singlet character,[1] although this is quite controversial and there is considerable evidence for "d-wave" pairing.[2–5] It is clear that magnetism exists near superconductivity, and many believe that magnetic fluctuations in some way mediate the pairing of carriers.[6–8] It is clear from both experiment[9] and first principles calculations[10–12] that the relevant copper and oxygen electronic states are strongly admixed through large hybridization matrix elements. At the same time, the copper states are strongly correlated with an effective (screened) on-site Coulomb repulsion of about 10 eV.[10,11,13]

No single theory accounts for all of these phenomena in a satisfactory way. Despite the strong theoretical bias towards single-band Hubbard or t-J models[14] which provide the hope of magnetically induced pairing, it is an open theoretical question as to whether these microscopic models indeed possess superconductivity of a robust enough character to explain the cuprates. The most recent results on the pure Hubbard model are discouraging,[15] while some hope is held out for the t-J model with large enough values of J (though it is not clear whether the relevant J values are realistic).[16] On the other hand, the Hubbard and t-J models have the virtue of building in strong correlations and magnetism, and certainly represent the simplest possible strongly correlated models for itinerant systems. It is therefore prudent to ask what other realistic physics might be added to these one-band models to allow for superconductivity.

There have been several proposals put forward based upon charge fluctuations.[17–21] That is, mechanisms in which virtual charge transfer serves as a "boson" to mediate the pairing of carriers. This generic pairing mechanism may also be regarded as "orbital fluctuation" mediated pairing since it always involves a transfer of charge between nearby electronic orbitals. Arguably the most notable charge fluctuation based mechanisms are those based upon (i) intersite, in-plane charge transfer between the copper d states and oxygen $p\sigma$ states[20] and (ii) intrasite copper charge transfer or quadrupolar fluctuations on the copper sites.[17–19] This paper shall present work based upon the latter suggestion.

In previous efforts on d-shell quadrupolar fluctuation mediated pairing, the fluctuations were treated as purely local in character, and the carriers were presumed to reside in the in-plane oxygen π orbitals.[17–19] Magnetic fluctuations on the copper sites were not treated explicitly within the model. Since interpretations of experimental data[22] and first principles calculations of electronic structure[10,11,13] strongly suggest that the doped holes go into bonding $p\sigma$ orbitals, it is clear that the earlier model calculations do not represent a very realistic treatment of quadrupolar fluctuation mediated pairing.

In order to investigate the possible relevance of quadrupolar fluctuation mediated pairing in a model which allows for copper magnetism, and which accounts in at least a virtual way for the oxygen-copper hybridization, we have studied a two-band Hubbard model which places x^2-y^2 and $3z^2-r^2$ levels on a two-dimensional square lattice corresponding to the cop-

0163-1829/94/49(2)/1255(14)/$06.00

per sublattice of the cuprates. All intersite hybridizations are treated as though arising from virtual hopping through the oxygen sites, and all Coulomb repulsions between on-site electrons are included. The interactions are treated perturbatively with self-consistency at the Hartree level. Instabilities are searched for with a full (though non-self-consistent) *dynamic* random-phase-approximation (RPA) treatment in which irreducible interactions for charge, magnetic, and superconducting instabilities are constructed from two-particle Green's functions. Our approach is patterned after the self-consistent (at the one-particle Green's function level) fluctuation exchange approximation used for the single-band Hubbard model.[7,23]

For realistic parameter values (which we discuss below) we find three kinds of instabilities in our model. First, in the doping region where the Fermi surface has predominant x^2-y^2 character, we find the conventional single-band Hubbard model magnetic instability, with associated d-wave superconductivity nearby.[24] In the region where the Fermi surface develops two sheets from overlapping bands of predominantly x^2-y^2 and $3z^2-r^2$ character, we find a superconducting instability clearly ascribed to interorbital fluctuations which are quadrupolar in this model. This instability has four notable features.

(i) There is no evidence for a nearby magnetic or charge instability within the full RPA analysis. This stands in contrast to the usual RPA result for the single-band model[7,23,24] and to the need in the intersite charge transfer scheme to fine-tune the charge transfer mediated pairing near a volume-collapse–charge-transfer instability.[20]

(ii) The RPA estimates for transition temperatures are as large as the magnetic fluctuation induced instabilities.

(iii) Both s-wave and d-wave pair states have similar energies at the instability boundary.

(iv) The instability persists in the absence of hybridization between the x^2-y^2 and $3z^2-r^2$ orbitals where it corresponds to a mixed pair state: One electron comes from the x^2-y^2 band and one from the $3z^2-r^2$ band. The pair state has d-wave symmetry as a result. The only process which can mediate such a state is interorbital fluctuations, which are predominantly local and have quadrupolar symmetry here. Indeed, the largest particle-hole susceptibility in this parameter region is the interband one. However, since it is interband pairing which dominates, the pairing must be highly spread in momentum and energy space. Thus, the effects come dominantly from an effective interaction highly localized in time and space. The reason is simple—it is impossible to construct zero momentum pairs which also have nearly zero energy or zero energy pairs which would also have zero momentum. An analysis restricted to the Fermi surface would thus miss this instability.

The study of multiband models is not new. The possibility of "pair hybridization" between different bands was studied by Suhl *et al.*[25] and more recently by Ihm and Lee[26] and, for interlayer pairing, by Chakravarty and coworkers.[27] In this scenario, Cooper pairs formed entirely within one band may hybridize through off-diagonal two-body interaction matrix elements with pairs from another band. The hybridization always enhances T_c independent of the sign by formation of bonding pair orbitals. This scenario is not relevant to the current paper, however, since it is readily seen that within a multiband Hubbard model, interband hybridization is required. Our instability persists even in the absence of interband hybridization. More relevant is the work on one-dimensional models[28] which studies pair correlations in a two-band model without interband hybridization by use of world line Monte Carlo techniques. The authors of Ref. 28 find a tendency towards interband pair formation. However, no extension of these calculations to dimensionality 2 or higher is possible due to the sign problem in the world line method. Our work, which we acknowledge to be approximate, may be regarded as presenting a scenario for interband pairing which may be examined by exact approaches or more sophisticated self-consistent perturbation theory schemes in the future.

We wish to emphasize that the RPA analysis contained in this paper overestimates the range of instability in the electron filling-temperature plane. Proper self-consistent inclusion of self energy corrections will renormalize the coupling strengths downwards, as we shall discuss in a later section in more detail, but they will note destroy the qualitative structure of the mean field phase boundary. Hence, the non-self-consistent RPA analysis is quite well suited for identifying parameter regimes in which to study the model with greater detail using exact approaches such as diagonalization and quantum Monte Carlo.

Since the realistic Fermi surfaces of relatively highly doped cuprates tend to have two sheets,[29,30] and in at least some cases one of the bands has been described as possessing significant $3z^2-r^2$ character,[12,30] we feel that our study should form the basis for more realistic investigations of the possibility that quadrupolar fluctuation mediated pairing is a viable mechanism for understanding the exotic superconductivity of the cuprates. It should be noted, however, that the data present a confusing picture of the amount of $3z^2-r^2$ character near the Fermi level: Core-level photoabsorption data suggest very little $3z^2-r^2$ occupancy in the ground state ($\leq 1\%$),[31] while NMR data suggest that some significant $3z^2-r^2$ charge transfer may take place as a function of doping.[32,33] In addition, optical evidence suggests the possibility that the $3z^2-r^2$ level may be as low as 0.3–0.4 eV above the x^2-y^2 level in the insulating phases of the cuprates.[34] Given these large experimental uncertainties, it is still prudent to entertain the possibility of quadrupolar fluctuation mediated pairing in the cuprates.

The paper is organized as follows: Section II describes the Hamiltonian in some detail and justifies the parameter choices. Section III describes the RPA method we have used which is based heavily on previous work by Bickers *et al.*[7,23] on the single-band Hubbard model, and by Littlewood *et al.* on the three-band Hubbard model with intersite charge transfer.[20] In Sec. IV we present the results of our calculations. In Sec. V we summarize and discuss future directions of the research which might spring from these results.

II. MODEL HAMILTONIAN

We have considered a two-band Hubbard Hamiltonian defined on a two-dimensional square lattice representing the copper sublattice of a copper oxide plane. At each site of the lattice we associate two electronic states, namely, the Cu $d_{x^2-y^2}$ and $d_{3z^2-r^2}$ states, which in the following will be denoted as x and z, respectively. In this model we are including the oxygen states only virtually in the sense that all the intersite hybridizations arise from virtual hopping through the oxygen atoms. The Hamiltonian is

$$H = H_0 + H_I \,, \tag{1}$$

where

$$H_0 = -t_{xx} \sum_{\langle ij\rangle\sigma} (d^\dagger_{ix\sigma} d_{jx\sigma} + \text{H.c.}) - t_{zz} \sum_{\langle ij\rangle\sigma} (d^\dagger_{iz\sigma} d_{jz\sigma} + \text{H.c.})$$
$$- t_{xz} \sum_{i\sigma} (d^\dagger_{ix\sigma} d_{i+\hat{x}z\sigma} + \text{H.c.} - d^\dagger_{ix\sigma} d_{i+\hat{y}z\sigma} + \text{H.c.} + x \leftrightarrow z) + \Delta \sum_i n_{ix} \tag{2}$$

and

$$H_I = \sum_i (U_{xx} n_{ix\uparrow} n_{ix\downarrow} + U_{zz} n_{iz\uparrow} n_{iz\downarrow} + U_{xz} n_{ix} n_{iz}) \,. \tag{3}$$

Here $t_{\alpha\beta}$ (α and β are used for the band indices x, z) are the hopping parameters. Notice that on-site xz hybridization is forbidden by the presumed tetragonal symmetry. The operators $d_{i\alpha\sigma}$ ($d^\dagger_{i\alpha\sigma}$) destroy (create) electrons in the α orbital at site i with spin σ. $U_{\alpha\beta}$ are the Coulomb interactions and $n_{i\alpha}$ the number operators for the site i and α orbital. The crystal field splitting Δ is defined as the energy difference between the centers of the x and z bands in the noninteracting limit with t_{xz} set to zero. The notation $\langle ij\rangle$ specifies nearest-neighbor summation.

The different terms and associated parameters which are included in this model Hamiltonian are described schematically in Fig. 1. In this figure we have also shown the electronic occupation for the "undoped system" (representing, e.g., La_2CuO_4), with the z band completely filled and the x band with a single electron per site. In order to reduce the parameter space of the model we took the three on-site Coulomb interactions to be the same, that is, $U_{xx} = U_{zz} = U_{xz} = U$, as also described in Fig. 1. We expect that this choice should not affect the qualitative picture which emerges from our results, even though in reality U_{xz} should be somewhat smaller than $U_{xx} = U_{zz}$. Furthermore, we assume that the three hopping parameters t_{xx}, t_{xz}, and t_{zz} are related via Slater-Koster theory:[35] In particular $t_{zz} = \frac{1}{3} t_{xx}$ and $t_{xz} = \frac{1}{\sqrt{3}} t_{xx}$.[36] Therefore we have a single independent hopping parameter. We have taken $t_{xx} = 1$ and all the energies in the problem are measured in unit of t_{xx}. We are left with two free parameters in the problem: U and the energy splitting Δ. Varying these (together with the occupancy n) sweeps us through the relevant physics regimes of the model.

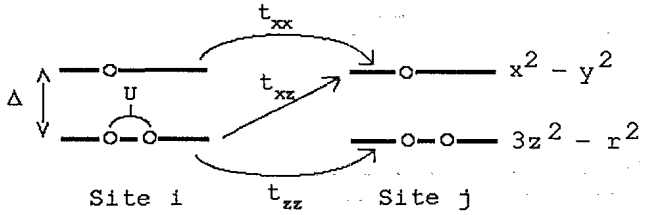

FIG. 1. Schematic representation of two-band Hubbard model. We show electronic energy levels for two neighboring sites (representing the square lattice copper sites of the CuO_2 planes in the cuprate superconductors) at a filling of n=3 electrons per site. This filling corresponds to the undoped La_2CuO_4 material. The highest level (half filled here) at the (bare) crystal field splitting Δ on each site has $x^2 - y^2$ symmetry; the lowest has $3z^2 - r^2$ symmetry. Hopping is possible between all levels as indicated, and we assume the magnitudes of the t_{xx} and t_{zz} integrals are determined by Koster-Slater arguments (Ref. 35). The Coulomb repulsion between all electrons on site has magnitude U.

Notice that by making Δ much larger than t_{xx} and putting the interband hopping integral $t_{xz} = 0$, we recover the single-band Hubbard model. We have studied this limit and we will show the comparison of our results with previous work on the single-band Hubbard model. This constitutes also a check of our code for the multiband model. We focused mainly on the study of the phase diagram of the two-band model Hamiltonian and in particular on how the properties of this model change as a function of the energy splitting Δ for a fixed value of the Coulomb repulsion U.

In most of our calculations we took $U/t_{xx} = 4$ which should be a reasonable value for copper oxide superconductors. In fact, the first principles estimates[10,11] yield U=10 eV, the copper-oxygen hopping matrix element t_{pd}=1.5–2.0 eV, and the copper-oxygen level splitting $\epsilon_p - \epsilon_d$ of 4 eV. From this information we estimate $t_{xx} \approx t_{pd}^2/(\epsilon_p - \epsilon_d) \approx 0.5$ eV.[36] This fixes U/t_{xx} at the much larger value of 20. However, the RPA greatly overestimates the tendency to an instability, and so a smaller U/t_{xx} value is likely to be more realistic. Moreover, the larger value would simply enlarge the phase boundaries in the T, n plane without altering the qualitative features. Hence, we have chosen to work with the smaller U/t_{xx} value in our work.

III. THEORETICAL APPROACH

In a recent work, Bickers *et al.*[7,23] have described a technique for investigating phase transitions and dy-

namics in interacting electron systems. Their approach is based on the numerical solution of a self-consistent conserving approximation for the self-energy. Within this approach the competition between different ordering transitions may be studied by solving numerically the Bethe-Salpeter equation within a discrete lattice (in momentum and frequency space). This approach has been applied to the single-band Hubbard model.[7] We have followed the same formalism in this work, although we have restricted the self-consistent calculation of the single-particle Green's functions at the Hartree-Fock level. These Green's functions are then used to compute the collective propagators that are needed to construct the irreducible interactions in the different scattering channels. Finally the Bethe-Salpeter equation is solved numerically to search for instabilities and to construct the phase diagram of the model.

A. Bare vertices

The possible scattering channels that we have to consider in order to construct the irreducible vertices are the particle-hole channel with total spin $S = 0$ (charge density ordering), the particle-hole channel with $S = 1$ (spin density ordering), the particle-particle channel with $S = 0$ (singlet superconductivity), and the particle-particle channel with $S = 1$ (triplet superconductivity). Following the notation of Bickers and Scalapino,[23] we shall use the labels d, m, s, t for bare interactions of charge, magnetic, singlet pair, and triplet pair excitations, while we shall use corresponding capital letters for the fluctuation exchange contributions (dressed by RPA theory fluctuations). In terms of these collective excitations, the interaction Hamiltonian may be written in a form that is easily utilized in the RPA, as described in Ref. 23. In our model, since we have two different bands, the bare vertices that constitute the basis of particle-hole and particle-particle pairs become 4×4 matrices. We associate by convention the index 1 to a xx pair, 2 to a xz pair, 3 to a zx pair, and 4 to a zz pair. For the particle-hole channel with $S = 0$ and $S = 1$, respectively, the bare vertices are

$$v_d = \begin{pmatrix} U & 0 & 0 & U \\ 0 & -U & 0 & 0 \\ 0 & 0 & -U & 0 \\ U & 0 & 0 & U \end{pmatrix}, \quad v_m = \begin{pmatrix} -U & 0 & 0 & 0 \\ 0 & -U & 0 & 0 \\ 0 & 0 & -U & 0 \\ 0 & 0 & 0 & -U \end{pmatrix}. \tag{4}$$

For the particle-particle channel the bare vertices are

$$v_s = \begin{pmatrix} U & 0 & 0 & 0 \\ 0 & U & 0 & 0 \\ 0 & 0 & U & 0 \\ 0 & 0 & 0 & U \end{pmatrix}, \quad v_t = \begin{pmatrix} 0 & 0 & 0 & 0 \\ 0 & U & 0 & 0 \\ 0 & 0 & U & 0 \\ 0 & 0 & 0 & 0 \end{pmatrix}. \tag{5}$$

It is important to stress some of the symmetry properties of the pair wave functions ϕ in the different channels. Each pair wave function has four sectors corresponding to the different band index combinations. Each sector carries the character of the anomalous expectation value attached to it ($d_{\alpha k_1 \sigma_1} d_{\beta k_2 \sigma_2}$). If α is different from β, we have to attach a $B_1(x^2 - y^2)$ character to that sector; otherwise for $\alpha = \beta$ the associated character is of $A_1(x^2 + y^2)$ symmetry.

B. Single-particle Green's function

We compute the single-particle Green's function self-consistently only within the Hartree-Fock approximation. As for the single-band Hubbard model the Fock term in the self-energy is identically zero. In particular the interband Fock term

$$\Sigma_{xz} = -\frac{U_{xz}}{N} \sum_{\mathbf{k},\omega} G_{xz}(\mathbf{k}, \omega) \tag{6}$$

is independent of $\mathbf{k}$ and ω. (N is the total number of $\mathbf{k}$ points or equivalently the number of lattice sites in a finite lattice.) But since this term has to transform like t_{xz} (i.e., like $x^2 - y^2$) the only possibility is that Σ_{xz} vanishes. The Hartree self-energy contains two contributions

$$\Sigma_{xx} = U_{xx} \frac{1}{2} n_x + U_{xz} n_z \,, \tag{7}$$

$$\Sigma_{zz} = U_{zz} \frac{1}{2} n_z + U_{xz} n_x \,. \tag{8}$$

Since we have taken all the Coulomb interactions to be the same, we get

$$\Sigma_{xx} = U(\tfrac{1}{2} n_x + n_z) \,, \tag{9}$$

$$\Sigma_{zz} = U(\tfrac{1}{2} n_z + n_x) \,. \tag{10}$$

The effect of the Hartree self-energy is a shift in the bare field splitting Δ. At a given electronic density $n = n_x + n_z$ the renormalized energy splitting is

$$\tilde{\Delta} = \Delta + (\Sigma_{xx} - \Sigma_{zz}) = \Delta + \frac{U}{2}(n_z - n_x) \,. \tag{11}$$

Using this value for $\tilde{\Delta}$, the renormalized energy bands in the diagonal representation are given by

$$E_{\pm}(\mathbf{k}) = \frac{1}{2}[\epsilon_{x\mathbf{k}} + \epsilon_{z\mathbf{k}} + \tilde{\Delta} \pm \sqrt{(\epsilon_{x\mathbf{k}} - \epsilon_{z\mathbf{k}} - \tilde{\Delta})^2 + 4\epsilon_{xz\mathbf{k}}^2}] \,, \tag{12}$$

where

$$\begin{aligned} \epsilon_{x\mathbf{k}} &= -2t_{xx}(\cos k_x + \cos k_y) \,, \\ \epsilon_{z\mathbf{k}} &= -2t_{zz}(\cos k_x + \cos k_y) \,, \\ \epsilon_{xz\mathbf{k}} &= -2t_{xz}(\cos k_x - \cos k_y) \end{aligned} \tag{13}$$

are the $\mathbf{k}$-space hopping matrix elements of the noninteracting energy bands.

In the diagonal representation the total density is given by

$$n(\mu, \tilde{\Delta}) = \frac{2}{N} \sum_{\mathbf{k}} [f(E_+(\mathbf{k})) + f(E_-(\mathbf{k}))] \,, \tag{14}$$

where $f(E)$ is the Fermi function. At a given total den-

sity n we find self-consistently the values of the chemical potential μ and of the energy difference $\tilde{\Delta}$ that are consistent with this n. The values of μ and $\tilde{\Delta}$ determined in this way are then used to compute the Hartree-Fock Green's functions given by the following equation:

$$G_{\alpha\beta}(\mathbf{k},\omega_n) = \begin{pmatrix} i\omega_n - \epsilon_{z\mathbf{k}} + \mu + \tilde{\Delta} & \epsilon_{xz\mathbf{k}} \\ \epsilon_{xz\mathbf{k}} & i\omega_n - \epsilon_{x\mathbf{k}} + \mu \end{pmatrix} \times \left[(i\omega_n - \epsilon_{z\mathbf{k}} + \mu + \tilde{\Delta})(i\omega_n - \epsilon_{x\mathbf{k}} + \mu) - \epsilon_{xz\mathbf{k}}{}^2 \right]^{-1} , \quad (15)$$

C. Irreducible interactions and the Bethe-Salpeter equation

By using the self-consistent single-particle propagator (with the Hartree approximation in this case) it is possible to compute the collective propagators that are needed for constructing the irreducible interactions in the various channels. Again because of the two-band indices the particle-hole and particle-particle susceptibilities are 4×4 matrices. In particular the particle-hole susceptibility is given by

$$\chi^{ph}_{\alpha\beta\gamma\delta}(\mathbf{q},\nu) = -\frac{\beta}{N}\sum_{\mathbf{k},\omega_n} G_{\alpha\gamma}(\mathbf{k}+\mathbf{q},\omega_n+\nu)G_{\delta\beta}(\mathbf{k},\omega_n) \quad (16)$$

and the particle-particle by

$$\chi^{pp}_{\alpha\beta\gamma\delta}(\mathbf{q},\nu) = \frac{\beta}{N}\sum_{\mathbf{k},\omega_n} G_{\alpha\gamma}(\mathbf{k}+\mathbf{q},\omega_n+\nu)G_{\beta\delta}(-\mathbf{k},-\omega_n) . \quad (17)$$

The sum over Matsubara frequencies can be performed analytically at this level of approximation for the Green's function. It can easily be shown (using conjugation and permutation properties of the single-particle Green's functions) that only 6 out of 16 elements of the susceptibilities are independent.

Following the generalized RPA formalism developed in Ref. 23 we can now write the irreducible vertices in the different channels. As noted above, bare interactions are denoted by lowercase v and lowercase collective excitation label d, m, s, or t, while fluctuation exchange contributions are denoted by lowercase v with uppercase D, M, S, T subscripts. Total interaction vertices are denoted by uppercase V with lowercase d, m, s, t subscripts. For the particle-hole with $S = 1$ channel (magnetic ordering) the irreducible vertex is given by

$$V_m = v_m + \frac{1}{2}v_D - \frac{1}{2}v_M + v_S - v_T , \quad (18)$$

for the particle-hole channel with $S = 0$ (charge density ordering) by

$$V_d = v_d + \frac{1}{2}v_D + \frac{3}{2}v_M - v_S - 3v_T , \quad (19)$$

and for the particle-particle channel with $S = 0$ (singlet superconductivity) by

$$V_s = v_s - \frac{1}{2}v_D + \frac{3}{2}v_M . \quad (20)$$

We omit discussion of triplet superconductivity since it appears to have no favorable regime in our model. In these equations the fluctuation exchange (RPA) contributions to the irreducible interaction vertices are defined as

$$v_M = v_m \frac{\chi^{ph}}{\hat{I} + v_m\chi^{ph}} v_m , \quad (21)$$

$$v_D = v_d \frac{\chi^{ph}}{\hat{I} + v_d\chi^{ph}} v_d , \quad (22)$$

$$v_S = v_s \frac{\chi^{pp}}{\hat{I} + v_s\chi^{pp}} v_s , \quad (23)$$

$$v_T = v_t \frac{\chi^{pp}}{\hat{I} + v_t\chi^{pp}} v_t , \quad (24)$$

where $\hat{I}$ is a 4×4 identity matrix and the above equations are understood to have implicit sums on momenta, energy, and band index.

We can investigate particle-hole and particle-particle instabilities using the Bethe-Salpeter equation again as described in Ref. 23. This corresponds to solving an eigenvalue problem for the matrix formed by the product of the irreducible interaction and the two Green's functions:

$$(-\beta V_r R)\phi = \lambda\phi , \quad (25)$$

where V_r is the irreducible vertex in a generic channel and R is the appropriate product of the two Green's functions. An instability of the normal state is signaled by the first appearance of a unit eigenvalue. For example, for the singlet superconductivity instability the Bethe-Salpeter equation is written as

$$-\sum_{\alpha'\beta'\gamma'\delta'\mathbf{k}'\omega'} V_{s,\alpha\delta'\gamma'\beta}(\mathbf{k}-\mathbf{k}',\omega-\omega')G_{\delta'\alpha'}(\omega',\mathbf{k}') \times G_{\gamma'\beta'}(-\omega',-\mathbf{k}')\phi_{\alpha'\beta'}(\omega',\mathbf{k}') = \lambda_s\phi_{\alpha\beta}(\omega,\mathbf{k}) . \quad (26)$$

For the magnetic instability the Bethe-Salpeter equation is

$$\sum_{\alpha'\beta'\gamma'\delta'\mathbf{k}'\omega'} [v_m + V^{ph}_{m,\alpha\delta'\beta\gamma'}(\mathbf{k}-\mathbf{k}',\omega-\omega') + V^{pp}_{m,\gamma'\alpha\delta'\beta}(\mathbf{k}+\mathbf{k}'+\mathbf{q},\omega+\omega')] \times G_{\delta'\alpha'}(\omega',\mathbf{k}'+\mathbf{q})G_{\gamma'\beta'}(\omega',\mathbf{k}')\phi_{\alpha'\beta'}(\omega',\mathbf{k}',\mathbf{q}) = \lambda_m\phi_{\alpha\beta}(\omega,\mathbf{k},\mathbf{q}) , \quad (27)$$

where we defined $V_m^{ph} = \frac{1}{2}(v_D - v_M)$ and $V_m^{pp} = v_S - v_T$. Finally, the Bethe-Salpeter equation for the charge density instability is

$$\sum_{\alpha'\beta'\gamma'\delta'\mathbf{k}'\omega'} [v_d + V^{ph}_{d,\alpha\delta'\beta\gamma'}(\mathbf{k}-\mathbf{k}',\omega-\omega') + V^{pp}_{d,\gamma'\alpha\delta'\beta}(\mathbf{k}+\mathbf{k}'+\mathbf{q},\omega+\omega')] \times G_{\delta'\alpha'}(\omega',\mathbf{k}'+\mathbf{q}) G_{\gamma'\beta'}(\omega',\mathbf{k}') \phi_{\alpha'\beta'}(\omega',\mathbf{k}',\mathbf{q}) = \lambda_d \phi_{\alpha\beta}(\omega,\mathbf{k},\mathbf{q}) , \quad (28)$$

where we defined $V_d^{ph} = \frac{1}{2}v_D + \frac{3}{2}v_M$ and $V_m^{pp} = -v_S - 3v_T$.

D. Numerical aspects

The self-consistent search for the chemical potential μ and for the renormalized energy splitting $\tilde{\Delta}$ can be mapped onto the problem of finding the minimum of a function of these two variables. Therefore standard minimization routines can be used for this aim and in particular we have used the Powell method.[38]

The numerical solution of the Bethe-Salpeter equation requires a discretization in momentum and frequency space. The Matsubara frequencies constitute a discrete set and we have used a cutoff in energy at about $\pm 8t_{xx}$. However, we found that the eigenvalues related to the superconducting instability are quite well converged even with a smaller cutoff (only four Matsubara frequencies are enough to get the eigenvalues converged well within 1% in the whole range of temperatures we have explored). The eigenvalues related to the magnetic or the charge density channel have instead a slower convergence with the energy cutoff (to get the same accuracy of 1% we need usually twice the number of Matsubara frequencies used for the superconducting instability). It is important to realize, as emphasized in Refs. 7 and 23, that the solution of the problem on a finite mesh in $\mathbf{k}$ space corresponds to an approximate discretization of the infinite lattice problem rather than to an approximate solution of the finite size in position space problem. Nonetheless, the discrete $\mathbf{k}$-space mesh gives information about position space correlations within a corresponding sized lattice region. We have used square lattices of 4×4, 8×8, and 16×16. The phase diagram that we report for our model is essentially unchanged in going from the 8×8 lattice to the 16×16 lattice. Therefore we believe that our results are not substantially affected by the numerical approximations in the solution of the Bethe-Salpeter equation.

We have solved the eigenvalue problem in two different ways: (i) using a direct diagonalization routine for the kernel of the Bethe-Salpeter equation; (ii) using an iterative scheme (projection technique) to extract the maximum eigenvalue of the matrix multiplying repeatedly the matrix on a trial vector with the appropriate symmetry. The latter method has the advantage that it does not require the storage of the entire matrix. However, this method yields only the maximum modulus eigenvalue of the matrix. In some cases we have found that the maximum modulus eigenvalue is negative in sign or a complex conjugate pair. When this occurs, one must make use of exact diagonalization or of another available iterative scheme that provide a larger set of eigenvalues. When possible we made use of the symmetry of the lattice to reduce sums over the Brillouin zone to only the irreducible wedge. This works for superconducting eigenvalues, but not for magnetic-charge instability eigenvalues where sums over the full zone are required.

IV. RESULTS

A. Single-band limit

To calibrate our approach to the two-band model, we first tested our programs in the single-band limit ($\Delta \to \infty$, $t_{zz} \to 0$). The phase diagram in this limit is presented in Fig. 2. The inset shows the phase diagram

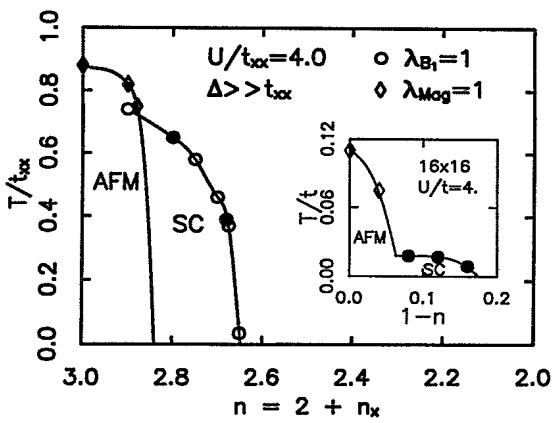

FIG. 2. Generalized RPA based temperature vs filling phase diagram of the two-band model in the single-band limit ($\Delta/t_{xx} \to \infty, t_{zz} \to 0$). The points represent instabilities determined by the temperature at fixed n for which the largest real Bethe-Salpeter eigenvalue (suitably normalized) is unity. Diamonds represent magnetic instability temperatures determined for an 8×8 mesh in $\mathbf{k}$ space. The magnetic instability always occurs for $\mathbf{q} = (\pi,\pi)$. (The line between the antiferromagnetic region and superconducting region is an extrapolation only.) Open (solid) circles represent calculated d-wave (B_1 symmetry) superconducting instability temperatures for 8×8 (16×16) mesh sizes. Note that the superconducting phase boundary is insensitive to the change in mesh size. The inset displays the corresponding results within the self-consistent fluctuation exchange approximation for a single-band Hubbard model of Ref. 7 in which the single-particle self energy is computed self-consistently. The resulting fluctuation corrections substantially reduce the instability region size in the $T-n$ plane, though the qualitative structure is similar to our results.

derived in Ref. 7 where the fully self-consistent program was used. There is excellent qualitative correspondence between the two phase diagrams. The magnetic instability occurs for $\mathbf{q} = (\pi, \pi)$ in each case. In each case, the superconducting pair wave function which first goes unstable is of d-wave (B_1) symmetry (though s-wave or A_1 pair wave functions become unstable at nearly the same temperature). The quantitative differences arise from the inclusion of self-energy corrections in the self-consistent scheme which reduce the instability temperatures by about an order of magnitude in the magnetic case and even more dramatically (a factor of 30) in the superconducting case. Moreover, the width of the region in n over which the instabilities occur is reduced with the self-energy corrections. These results are consistent with the statements about the effects of full self-consistency made in Ref. 7.

The strong suppression of the phase boundary with self-consistency is not surprising. The dominant effect of the self-energy inclusion is expected to be renormalization of the dimensionless electron-electron coupling constant. For example, as is well known in the strong coupling theory for conventional superconductors, self-consistency which includes the wave function renormalization factor $Z(\omega) = 1 - \partial\Sigma(\omega)/\partial i\omega$ has the approximate effect of replacing the dimensionless electron-phonon coupling strength λ by $\lambda/(1+\lambda)$. A superconducting transition is found over the entire range of λ, however, provided the renormalized attractive coupling exceeds the renormalized (retardation reduced) Coulomb interaction.[37] In the case of the Hubbard model treatment here, all repulsive and attractive interactions are included prior to renormalization, and so the renormalization will not be expected to affect the sign of the net dimensionless coupling, only the magnitude. Thus we do not expect the strong coupling corrections to modify the conclusion that within RPA we will have a superconducting instability.

B. Two-band limit

We now turn to the principal results of this work, which are found in the two-band limit when there is a significant overlap between the two bands. We tried several values of Δ, and found that when $\Delta \geq 5$ we revert to the single-band limit for the upper band with occupancy $2 \leq n \leq 4$. This is sensible, since the bands are well separated in comparison to the respective widths. The interesting physics arises when we take $\Delta \approx 1$. In this case, we see a changeover from single-band-like behavior near $n = 3$ to intrinsically different two-band behavior near n=2. We note that the Hartree shifted value of the crystal field splitting is substantially larger than 1 in this region ($\tilde{\Delta} \approx 3.3$ at the instability temperature). Nevertheless, the quadrupolar fluctuation mediated superconductivity persists due to significant overlap of the band of dominant x character with that of dominant z character.

The phase diagram for the case $\Delta = 1$ is shown in Fig. 3. The significant features are as follows: (i) Near $n = 3$, we see magnetic and superconducting instabilities qualitatively and quantitatively similar to those of Fig. 2 which is the true single-band limit. As in Fig. 2, the

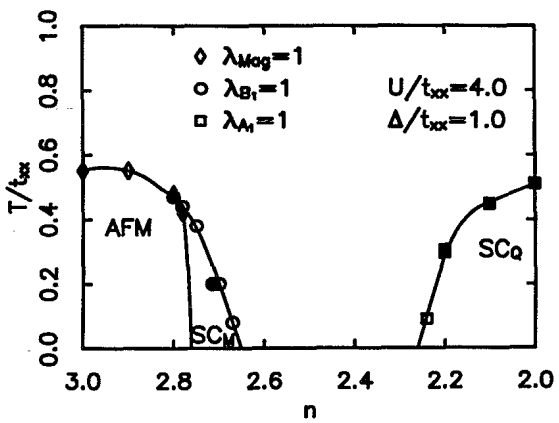

FIG. 3. Generalized RPA based temperature vs filling phase diagram of the two-band model in the overlapping band limit ($\Delta = 1.0$). Symbols near n=3 are the same as in the previous graph; clearly the behavior near n=3 is reminiscent of the single-band limit and the superconductivity (SC_M) is induced by magnetic fluctuations. Near n=2, we have a qualitatively different region of superconductivity (SC_Q) associated with quadrupolar fluctuations—here open (solid) squares represent the Bethe-Salpeter instability temperature for an 8×8 (16×16) **k** mesh. Note that the pair wave function symmetry of the SC_M phase at the instability is always d wave (B_1), while for $n > 2$ the instability of the SC_Q phase has A_1 (s-wave) symmetry. (At n=2, A_1 and B_1 states have near degeneracy, with B_1 slightly favored.) Notice that the instability boundaries are almost unchanged with the increased lattice size.

magnetic instability always occurs for $q = (\pi, \pi)$, and the leading superconducting instability has d-wave symmetry. (As we shall discuss below, the magnetic instability yields this result despite no significant nesting features on the Fermi surface.) (ii) There is a gap in occupancy between approximately 2.7 and 2.25 in which no instability is manifested—while we find evidence for superconducting instabilities for small **k**-space mesh sizes, the transition temperatures scale to zero as we increase the mesh size. In contrast, the instabilities near n=2,3 are quite stable with respect to change in mesh size. (iii) The principal result of this work is the region of superconducting instability centered about n=2. As we shall discuss, this instability is clearly associated with interband charge transfer of local quadrupolar character (the interband susceptibility χ_{xz} is the largest here). Moreover, in contrast to the single-band-like results near n=3, there is no proximity to a charge or magnetic instability. This makes the character of this charge transfer mediated superconductivity very different from that of the intersite charge transfer mechanism.[20] This result also implies that the model cannot be mapped to an effective negative-U Hubbard model, for which charge density wave and superconducting instabilities are close together.[39] (iv) Finally, we find that the s-wave (A_1) and d-wave (B_1) symmetry pair wave functions become unstable at essentially the same temperature and have significant contributions from other than nearest-neighbor pair form factors in real space. The overlap of the bands in this region and the essential degeneracy of d-wave and s-wave superconductiv-

ity may have significant phenomenological implications, as we shall discuss later.

C. Origin of the superconducting instability: Interorbital quadrupolar mediated pairing

Static susceptibilities. In order to justify the identification of the new superconducting instability we have found with a quadrupolar character fluctuation from x^2-y^2 to $3z^2-r^2$ orbitals, we shall first examine the static susceptibilities computed within the Hartree approximation. Figure 4 shows the particle-hole susceptibilities for particle-hole pairs of xx symmetry and xz symmetry at the fixed temperature of 0.5, near to the maximum instability temperatures we have computed. For $2.5 \leq n \leq 3.0$, we find that the intraband xx susceptibility dominates, and as n is lowered from 3, the q value at which it is maximum moves continuously from the zone corner along the zone boundary towards $(\pi, 0)$ within the irreducible wedge. For $2.0 \leq n \leq 2.5$, the dominant susceptibility becomes the interband susceptibility associated with quadrupolar fluctuations, χ_{xz}. This susceptibility (except near n=2.5) has a peak always at (π, π). Note that for the value of U chosen, this susceptibility almost drives Stoner-criterion magnetic and charge instabilities, i.e., instabilities of the RPA with the irreducible interaction approximated by the bare vertex. However, inclusion of the fluctuation corrections to the irreducible interaction removes completely any tendency towards magnetic or charge instabilities. Note that as n is decreased further below 2.0, the maximum value of χ_{xz} begins to monotonically drop followed by a dominance of χ_{zz} and a single-band-like picture for the predominantly z-character states.

Charge transfer. In addition to the growth of the interband susceptibility, we find significant charge transfer from x to z orbitals in the region where the quadrupolar fluctuation mediated superconducting instability becomes important. This is illustrated in Fig. 5(b) where the occupancies of x and z orbitals are plotted vs the total occupancy (their sum) at the temperature T=0.5 used in Fig. 4. It is clear that near n=2.4, a break occurs in the n_z occupancy; in the same region, the occupancy n_x is relatively flat with n. In contrast, in Fig. 5(a) we display what is essentially a single-band limit effected by taking Δ to 5.0. In that case, the n_z occupancy is completely constant at as n is lowered from 3.0 to 2.0, while the n_x occupancy drops continuously from 1.0 to 0. Thus, at the maximum instability temperature for the quadrupolar fluctuation mediated superconductivity, the *hole occupancy* $3-n$ in our model calculation is shared nearly equally by the x and z orbitals.

Pairing symmetry, zero hybridization limit. To further test the assignment of this pairing to interorbital quadrupolar fluctuations, we have examined the symmetry of the B_1 and A_1 pairing components. These are energetically close over the entire range of occupancy values. The B_1 state has a dominant mixed pair component with one member from the x and one from the z band. Indeed, the B_1 state is actually more stable *when the $x-z$ hybridization is set to zero*, while the eigenvalue of the A_1 state becomes very small in that limit

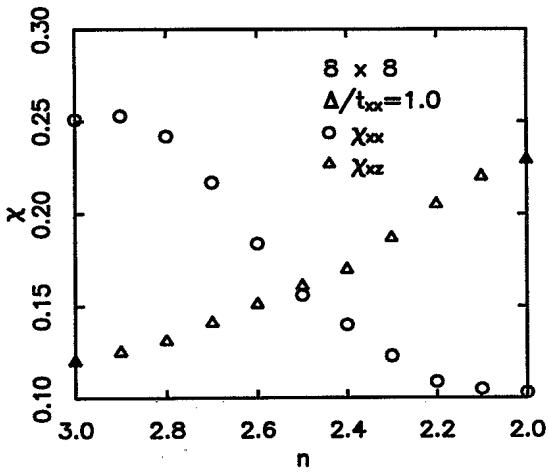

FIG. 4. Evolution of static particle-hole susceptibility as a function of filling for the overlapping band limit of the two-band model ($\Delta = 1.0$, $T = 0.5$). We have plotted the maximum values (over the Brillouin zone) of the static susceptibilities of xx and xz character. For $2.5 < n < 3.0$, the susceptibility of xx character dominates—this mainly arises from intraband processes in the upper band. The **q** value at which this peak is located evolves continuously from (π, π) at n=3 down the Brillouin zone boundary. For $2.0 < n < 2.5$ the largest susceptibility had dominant xz character arising primarily from interband transitions. The **q** value at which χ_{xz} peaks is (π, π) for $n < 2.4$.

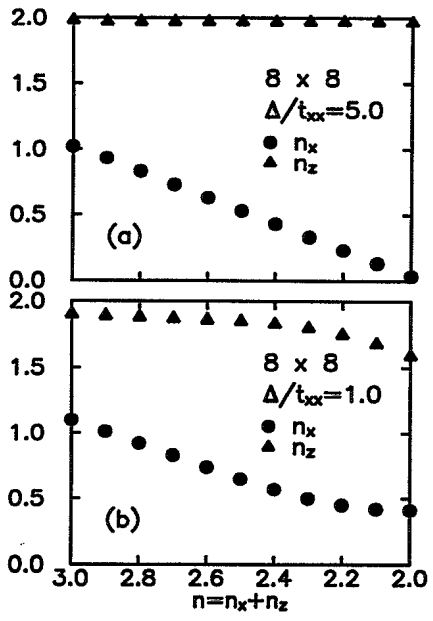

FIG. 5. Occupancies of $x(n_x)$ and $z(n_z)$ levels as a function of total occupancy n for the two-band model. For both (a) and (b) we take $T = 0.5$. (a) illustrates results for the large Δ ($\Delta = 5.0$) limit which is effectively a single-band model. Note the monotonic decrease of n_x and the complete constancy of n_z as a function of n. (b) illustrates results for $\Delta = 1.0$ which shows a flattening in the n_x curve near n=2.3; at the same occupancy, n_z begins to curve downwards rather sharply. This demonstrates significant charge transfer between the levels.

(not shown). We find the maximum T_c enhanced in this limit with dominant B_1 symmetry. A simple diagram (see Fig. 6) shows that for $t_{xz} = 0$, interband pairing is possible only via exchange of orbital fluctuations (at lowest order). We stress that the B_1 symmetry pairing, of possible phenomenological relevance to the cuprates, is only possible because of the orbital symmetry present in this model.

Quadrupolar fluctuations: symmetry considerations. It is reasonable to question a description of the orbital fluctuations as quadrupolar in this case since, strictly speaking, the quadrupolar fluctuation operator has a unique symmetry identification only at the Brillouin zone center and corner. It will mix, for example, with the charge density operator at arbitrary points in the Brillouin zone. However, since the largest value for χ_{xz} occurs at zone corner, the dominant fluctuations will occur near there where the quadrupolar label is sensible.

Clearly, for the U values we study here, we are somewhere between weak and strong coupling. Given that our χ_{xz} results are rather independent of $\mathbf{q}$ (though peaked at the zone corner) a local description is apparently appropriate. In such a local description, the on-site interorbital fluctuation is clearly quadrupolar in character, and such a description is not vacuous since it implies detailed symmetry information not present in a description as "interorbital fluctuation." For example, as mentioned earlier, the mixed xz component of the pair wave function has a B_1 symmetry which is not the generic case for arbitrary orbital choice. Hence we feel that the identification of the pairing mechanism with quadrupolar fluctuations is quite appropriate.

D. Fermi surface

Having made the identification of the superconducting instability as being mediated by quadrupolar fluctuations with an associated $x \rightarrow z$ charge transfer, we now discuss the character of the Fermi surface in our model calculations as a function of doping n. These results are displayed in Fig. 7. At n=3.0, a single Fermi surface sheet is present, which has mostly x-orbital character and is centered at Γ. (This feature clearly evolves in an electronlike way with doping, in contrast to the observations of photoemission.[29] We attribute this discrepancy to the extreme simplicity of our two-band model.) Note that despite the similarity of the phase diagram in this region to that of the single-band model, there is *no* nesting of the Fermi surface at n=3.0. As a function of n, the x-like, Γ-centered sheet continuously shrinks in size (see the n=2.2 plot). Finally, near n=2.1, a new holelike sheet arises at the M point (zone corner) of the Brillouin zone which has significant z character. Note that, consistent with the flatness of n_x below $n = 2.2$ [cf. Fig. 5(b)], the area

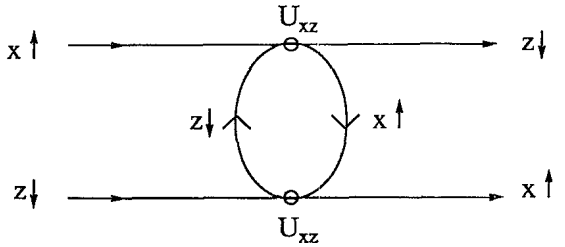

FIG. 6. Interband pair interaction diagram for t_{xz}=0. In this diagram, orbital and spin labels are exchanged for an incoming mixed band pair. This diagram is nonzero even for $t_{xz} = 0$.

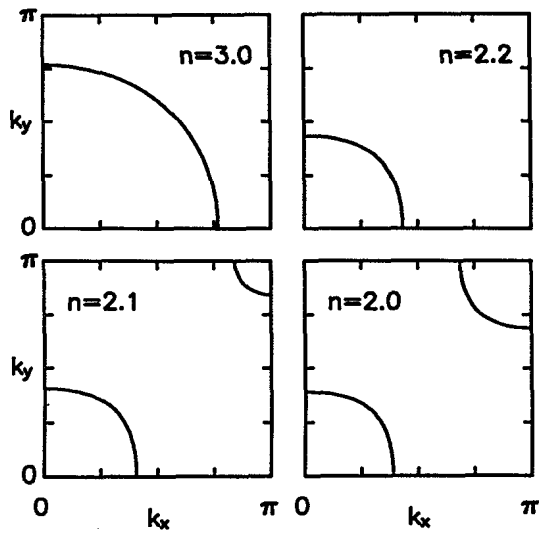

FIG. 7. Evolution of the Fermi surface as a function of doping n in the overlapping band limit ($\Delta = 1.0$). For n=3 only one sheet of x character is visible; this is electronlike within the calculation and centered at the Γ point. For n=2.2 the size of this sheet is significantly reduced and remains roughly constant in area as n is lowered further, consistent with the results of Fig. 5. For $n < 2.2$, a second feature of hole character centered at the zone-corner (M) point arises; this feature has mostly z character. We note that the development of quadrupolar fluctuation mediated pairing of Fig. 3, the growth of the mixed susceptibility χ_{xz} (see Fig. 4), and the charge transfer from $x \rightarrow z$ of Fig. 5 arise roughly concomitantly with this second Fermi surface sheet.

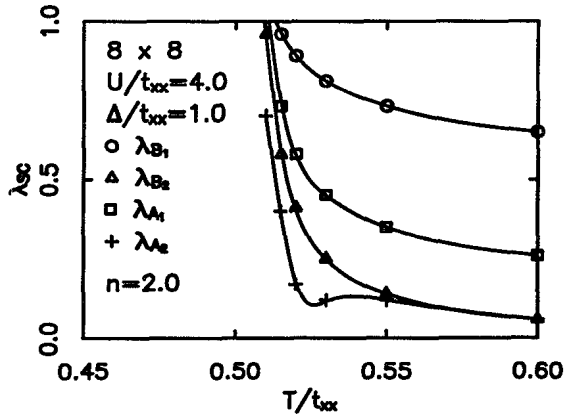

FIG. 8. Bethe-Salpeter superconducting instability eigenvalues λ_{SC} for the two-band model in the overlapping band limit ($\Delta = 1.0$). The eigenvalues are shown for the 8×8 lattice at the doping level (n=2) which provides the maximum instability temperature within this approach. We note B_1, A_1, and B_2 eigenvalues reach unity (signaling the instability) at nearly the same temperature. For somewhat larger n, the A_1 symmetry eigenvalue reaches unity first.

enclosed by the Γ-centered sheet is relatively insensitive to doping below n=2.2. It is intriguing that it is in this region where the two Fermi-surface sheets arise in which we find the strongest quadrupolar fluctuation mediated superconductivity. We note that the electron doped side ($n > 3.0$—not shown) displays a similar phase diagram as n is increased to the hole doped phase diagram as n is decreased. However, there is no quadrupolar fluctuation mediated region in the $n > 3$ region—this requires overlap of the two bands near the Fermi surface which is clearly not possible with electron doping.

E. Quadrupolar fluctuation mediated superconductivity

We now turn to a discussion of the quadrupolar fluctuation mediated superconductivity. Figure 8 displays the Bethe-Salpeter eigenvalues for the various pair wave function symmetries at n=2.0. It is clear that the s-wave (A_1) and d-wave (B_1) symmetry states are essentially degenerate—i.e., they both become unstable near the same temperature. It is also clear that the B_2 (xy) symmetry and A_2 [$(xy)(x^2 - y^2)$] symmetry states are

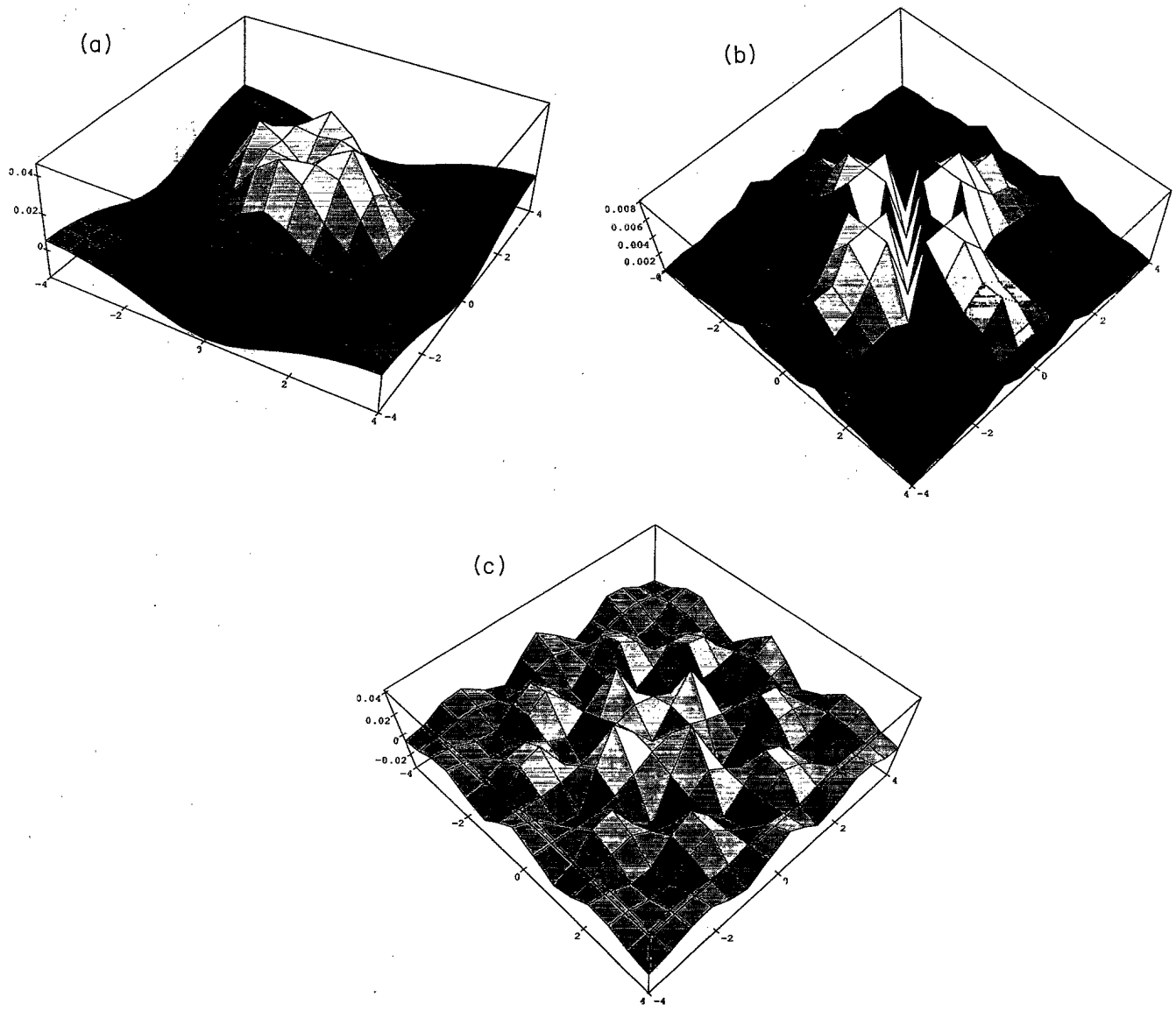

FIG. 9. Real space form factor of the unstable A_1 symmetry Bethe-Salpeter superconducting eigenvector in the overlapping band limit ($\Delta = 1.0$, $n = 2.0$, $T = 0.51$). All form factors are displayed for the lowest Matsubara frequency available and for an 8×8 lattice. (a) shows the xx-sector result, which has most weight at nearest-neighbor positions. (b) shows the modulus of the xz-sector form factor, which has B_1 symmetry to offset the intrinsic B_1 symmetry of the anomalous xz amplitude; this form factor has significant nearest-neighbor weight, but considerable weight at third neighbor positions as well. (c) shows the zz-sector form factor which has nearly equal weight at first, second, and third neighbor sites, and comparable integrated intensity to the xx-sector form factor.

relatively close in energy as well, though somewhat less prone to instability. In fact, this appears to be a generic feature whenever we find a superconducting instability in this approach—as one singlet pair state goes unstable, the rest seem to follow suit closely. For occupancies greater than 2, the quadrupolar mediated superconductivity slightly favors A_1 symmetry states, with both B_1 and B_2 symmetries nearby in energy.

It is of considerable interest to discuss the real space form factors of our unstable pair states since they are rather unusual and would be difficult to access in the state of the art Monte Carlo and exact diagonalization studies[40] which have typically considered pair instabilities on lattices no larger than 4×4. Figure 9(a) displays the form factor of the xx sector of the unstable Bethe-Salpeter pair eigenvector for A_1 symmetry at the lowest Matsubara frequency (the amplitudes of the eigenvectors fall off sharply with increasing Matsubara frequency). As might be expected, given the large on-site repulsion, most of the weight appears on nearest-neighbor sites. However, there is significant weight in the tails of the wave function near $\mathbf{R} = (4, 0)$, for example. The *modulus* of the xz sector of the unstable A_1 symmetry eigenvector is plotted in Fig. 9(b). As expected, since this sector has a form factor with $x^2 - y^2$ symmetry nodal surfaces due to the B_1 character of the anomalous expectation value, there is no weight at the origin and significant weight at nearest-neighbor sites along the x and y directions, but also relatively long tails along the x and y directions. Figure 9(c) displays the zz sector form factor of the A_1 eigenvector. Despite the lower intensity of individual peaks relative to the xx sector, the greater number of peaks gives an

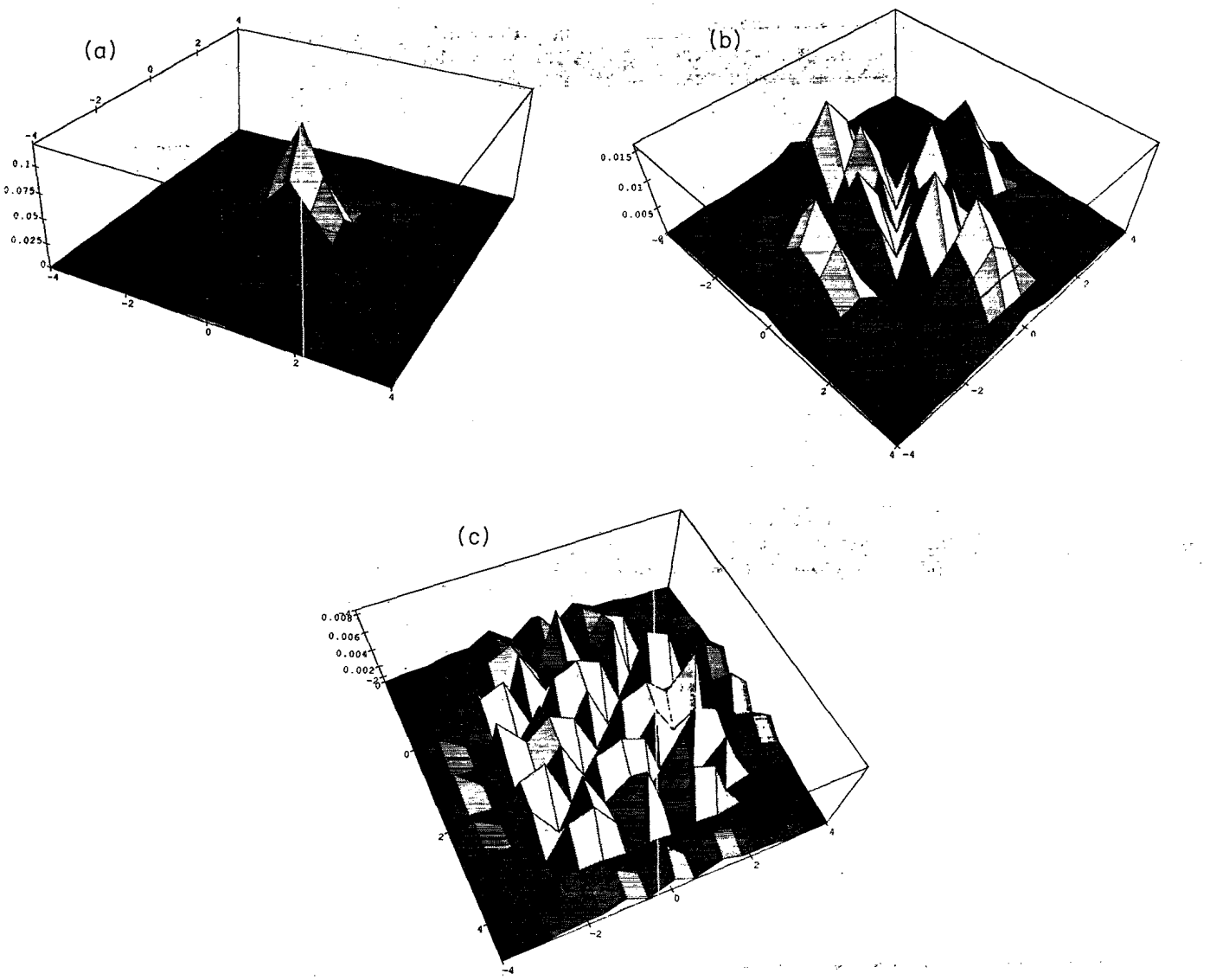

FIG. 10. Real space form factor of the unstable B_1 symmetry Bethe-Salpeter superconducting eigenvector in the overlapping band limit ($\Delta = 1.0$, $n = 2.0$, $T = 0.51$). All form factors are displayed for the lowest Matsubara frequency available and for an 8×8 lattice. The greatest weight in this case appears in the xz-sector form-factor modulus shown in (a), which has A_1 symmetry because of the intrinsic B_1 symmetry of the anomalous xz amplitude. Note that most of the xz weight appears on site. (b) shows the xx-sector result, which has equal weight peaks at nearest and third nearest-neighbor positions. (c) shows the zz-symmetry form factor which has weight spread over a wide range.

integrated intensity comparable to that of the xx sector. Note also that the zz weight is spread out nearly equally over first, second, and third neighbor sites.

We note that the relatively long decays of the real space form factors cannot be detected by finite size calculations utilizing 4×4 lattices. The reason is simple: The irreducible wedge of such a lattice has only six points and is most sensitive to nearest-neighbor form factor variations which possess one radial node. The oscillations apparent in Fig. 9 require more irreducible wedge points to pick out the greater number of radial nodes. It is for this reason, for example, that the Monte Carlo study of Ref. [40] may contain an artificially suppressed B_2 symmetry pair instability—because of the nodal structure of that state, only the $(\pi/2, \pi/2)$ point in the wedge could yield nonvanishing contributions for the 4×4 lattice and this small phase space led to what we feel may be incorrect estimates of the relevance of the B_2 state.

Figures 10(a–c) display the real space pair form factors for the xx, zz, and xz sectors of the B_1 symmetry unstable Bethe-Salpeter eigenvector for n=2.0. In this case, the dominant intensity resides in the xz sector [Fig. 10(a)]. This has almost all intensity localized at the origin (the form factor here has A_1 symmetry since the anomalous expectation value has B_1 symmetry). We find similar results when $t_{xz} = 0$ as discussed below. The xx sector modulus is plotted in Fig. 10(b); since this form factor has B_1 symmetry, its intensity is concentrated along the x and y directions, with nearly equal weight at nearest-neighbor and third nearest-neighbor positions. Finally, the modulus of the zz sector has, similar to Fig. 9(b), weight spread significantly in real space over first, third, and fifth neighbor positions (reflecting the B_1 nodal structure). As commented in the previous paragraph, the significant real space variation of the xx and zz sectors would be missed in finite size studies on 4×4 lattices.

We note that since the dominant component of the xz pairing occurs *on site*, this further strengthens the assignment of the mechanism to quadrupolar fluctuations, which have a well-defined symmetry content at a single site. However, the pairing clearly has to be strongly spread in energy and momentum, since one cannot simultaneously satisfy the requirements of zero momentum for an interband pair *and* zero energy. Indeed, for $t_{xz} = 0$ we find the structure of the eigenvector corresponding to the largest eigenvalue to be dispersed in magnitude by about 3% in momentum space and falling off with a characteristic energy of order the bandwidth in Matsubara frequency space. This result is surprising given the large on-site Coulomb interaction between xz orbitals. We note that our analysis accounts both for fluctuation mediated attraction and the instantaneous repulsion.

V. CONCLUSIONS AND SUMMARY

Obviously this model is too simple to be more than a caricature of the full behavior present in the copper oxide superconductors. In particular, we have not explicitly included the oxygen bands in this work, a point which we shall elaborate on below. Nevertheless, this paper presents an extensive study of the possible role of quadrupolar fluctuations within an itinerant framework, and the results of the calculations suggest several phenomenological connections to the cuprates.

First, we note that the quadrupolar fluctuations occur most strongly in a region where the Fermi surface has two sheets. Two sheets are qualitatively consistent with the data for $YBa_2Cu_3O_{7-\delta}$ and $Bi_2Sr_2CaCu_2O_{8+y}$.[29,30] Moreover, the second sheet is expected to contain significant z character as has emerged in electronic structure calculations.[12] It is interesting that the superconductivity correlates with significant $x \rightarrow z$ charge transfer since one interpretation of polarized L_{III} core-level absorption spectra at the copper sites promotes just this picture.[41] This interpretation has been strongly questioned more recently, though.[31] In this region of doping our model produces the wrong curvature for the x-like sheet, and requires an overall filling of $n = 2$, far less than the estimated $n = 2.6$–2.7 in, say, $YBa_2Cu_3O_{7-\delta}$. However, the omission of the other (oxygen-derived) bands in the calculation is likely to seriously adjust both the curvature and occupancy estimates without modifying the above qualitative features. After all, the electronic structure calculations which reproduce the Fermi surfaces accurately place significant z weight at or near the Fermi surface.[12]

Second, we note that the asymmetry of the phase diagram with respect to electron and hole doping may be of relevance in the following sense: In the hole doped materials, the superconducting transition temperature may rise to values as large as 125 K in the three-layer systems. This suggests that a different mechanism may be involved in producing the superconductivity for the electron doped materials. Moreover, the electron doped materials possess a region of superconductivity as a function of doping which abuts the magnetic transition—in the hole doped materials they are well separated.

Finally, we observe that the proximity of the s-wave (A_1) and d-wave (B_1) symmetry instabilities is more pronounced in the region of quadrupolar fluctuation mediated pairing than the single-band-Hubbard-like region near n=3. The potential significance of this result is that s-wave and d-wave states may couple to produce $s + id$ states[42,43] which allows reconciliation of various experimental data such as the absence of the Hebel-Slichter relaxation peak in NMR (favoring d-wave pairs) with the apparent s-like character stressed in muon spin relaxation measurements of the penetration depth.[44] If the character of the order parameter were d wave at the transition but then the system crossed over to $s + id$-wave behavior at lower temperatures, this apparent discrepancy could be possibly resolved—the $s + id$ state always has a net gap.

We would like to stress that our work is a pass at the problem from this framework. There are two main directions in which future work needs to go. First, it is important to include the self-consistent self-energy corrections to the model since, as mentioned in the discussion of the single-band limit, these corrections may reduce transition temperatures by an order of magnitude or more and narrow the window of occupancy in which

the superconducting and magnetic instabilities may occur. Of particular interest is whether the quadrupolar mediated pairing instability is less sensitive to these corrections than the magnetic fluctuation mediated pairing instability of the single-band model. Second, it is important to include the oxygen σ bands explicitly. These are likely to modify some of the features derived in our calculations as mentioned above.

It is interesting to speculate, given the highly local character of the interband pairs identified for t_{xz}=0, whether the interorbital fluctuations may not lead to a bipolaron in more sophisticated treatments of the model.

In summary, we have computed phase diagrams within a generalized RPA approximation for a two-band Hubbard model of the copper oxide superconductors. This model includes both quadrupolar and magnetic fluctuations on an equal footing, and allows for significant offsite admixture of the x and z states. These features were omitted from previous studies of quadrupolar fluctuation mechanisms in the cuprates. We find that when the bare crystal field splitting Δ on the copper sites has the realistic value of 1 (in units of the effective xx hopping t_{xx}), single-band-Hubbard-like behavior occurs near n=3. In addition, we have found a qualitatively new superconducting instability at reduced electron concentration ($n \approx 2$) which is clearly associated with quadrupolar fluctuations and $x \rightarrow z$ charge transfer. Unlike the magnetic fluctuation mediated pairing found within RPA in the single-band model, and unlike the intersite charge transfer mediated pairing of the three-band model, this quadrupolar fluctuation mediated pairing has no nearby particle-hole instability. Moreover, in this doping region there are two Fermi-surface sheets in agreement with photoemission, positron annihilation, and de Haas–van Alphen data on the two-layer superconducting systems. The A_1 superconducting state has a real space form factor with significant extent beyond nearest neighbors, and both A_1 and B_1 symmetries have nearly the same transition temperatures. The B_1 symmetry state is most stable for zero interband hybridization ($t_{xz} = 0$) where it is comprised of mixed band pairs. This indicates a pairing state highly spread in energy and momentum space. A simple Fermi surface averaging would miss the pairing. These facts may be of relevance to the phenomenological understanding of the superconducting state properties of these exotic materials.

ACKNOWLEDGMENTS

We would like to acknowledge useful discussions with J. W. Wilkins. We are especially grateful to N. E. Bickers for many useful discussions about the fluctuation exchange approximation used here and in his work, and for sharing his computer codes for the single-band model. This work was supported by grants from the U.S. Department of Energy, Office of Basic Energy Sciences. Supercomputer computations were carried out on a grant of time from the Ohio Supercomputer Center.

*Present address: IBM European Center for Scientific and Engineering Computing, Viale Oceano Pacifico 171, I-00144 Rome, Italy.

[1] An excellent overview is contained in *High Temperature Superconductivity,* The 1989 Los Alamos Symposium, edited by K.S. Bedell *et al.* (Addison-Wesley, Redwood City, 1990).

[2] See, for example, J. Annett, N. Goldenfeld, and S.R. Renn, Phys. Rev. B **43**, 2778 (1991).

[3] S.E. Barrett, J.A. Martindale, D.J. Durand, C.H. Pennington, C.P. Slichter, T.A. Friedmann, J.P. Rice, and D.M. Ginsburg, Phys. Rev. Lett. **66**, 108 (1991).

[4] W.N. Hardy, D.A. Bonn, D.C. Morgan, R. Liang, and K. Zhang, Phys. Rev. Lett. **70**, 3999 (1993).

[5] Z.-X. Shen, D.S. Dessau, B.O. Wells, D.M. King, W.E. Spicer, A.J. Arko, D. Marshall, L.W. Lombardo, A. Kapitulnik, P. Dickinson, S. Doniach, J. DiCarlo, A.G. Loeser, and C.H. Park, Phys. Rev. Lett. **70**, 1553 (1993).

[6] See, for example, the review by D.L. Cox, in *High T_c Superconducting Thin Films: Processing, Characterization and Applications (Boston, MA, 1989)*, Proceedings of meeting to draw together researchers from a range of fields and to provide a forum for the exchange of ideas between related areas of research (processing, characterization, and applications), edited by Roger L. Stockbauer, S.V. Krishnaswamy, and Richard L. Kurtz, AIP Conf. Proc. No. 200 (AIP, New York, 1989), p. 3.

[7] N.E. Bickers, D.J. Scalapino, and S.R. White, Phys. Rev. Lett. **62**, 961 (1989).

[8] P. Monthoux and D. Pines, Phys. Rev. B **47**, 6069 (1993).

[9] A. J. Arko *et al.*, Phys. Rev. B **40**, 2268 (1989).

[10] A.K. McMahan, R.M. Martin, and S. Satpathy, Phys. Rev. B **38**, 6650 (1988).

[11] M. Hybertsen, M. Schluter, and N.E. Christensen, Phys. Rev. B. **39**, 9028 (1989).

[12] S. Massidda, J. Yu, and A.J. Freeman, Physica C **152**, 251 (1988).

[13] J.B. Grant and A.K. McMahan, Phys. Rev. Lett. **66**, 488 (1991).

[14] See, for example, P.W. Anderson and J.R. Schrieffer, Phys. Today **44** (6), 55 (1991).

[15] M. Imada (unpublished).

[16] See, for example, H. Yokoyama and M. Ogata (unpublished).

[17] W. Weber, Z. Phys. B **70**, 323 (1988); Y.B. Gaidedey and V.M. Loktev, Phys. Status Solidi B **147**, 307 (1987).

[18] D.L. Cox, M. Jarrell, C. Jayaprakash, H.R. Krishnamurthy, and J. Deisz, Phys. Rev. Lett. **62**, 2188 (1989).

[19] M. Jarrell and D.L. Cox, Phys. Rev. B **42**, 7960 (1990).

[20] P.B. Littlewood, C.M. Varma, and E. Abrahams, Phys. Rev. Lett. **63**, 2602 (1989).

[21] A. Georges, G. Kotliar, and W. Krauth (unpublished).

[22] M. Takigawa, P.C. Hammel, R.H. Heffner, Z. Fisk, K.C. Ott, and J.D. Thompson, Phys. Rev. Lett. **63**, 1865 (1989).

[23] N.E. Bickers and D.J. Scalapino, Ann. Phys. (N.Y.) **193**, 206 (1989).

[24] D.J. Scalapino, E. Loh, Jr., and J.E. Hirsch, Phys. Rev. B **34**, 8190 (1986).

[25] H. Suhl, B.T. Matthias, and L.R. Walker, Phys. Rev. Lett. **3**, 552 (1959).

[26]D.H. Lee and J. Ihm, Solid State Commun. **62**, 811 (1987).
[27]S. Chakravarty, A. Sudbo, P.W. Anderson, and S. Strong (unpublished).
[28]H. Aoki and K. Kuroki, Phys. Rev. B **42**, 2125 (1990).
[29]J.C. Campuzano *et al.*, Phys. Rev. Lett. **64**, 2308 (1990).
[30]J.L. Smith, C.M. Fowler, B.L. Freeman, W.L. Hults, J.C. King, and F.M. Mueller, in *Proceedings of University of Miami Workshop on Electronic Structure and Mechanisms for High Temperature Superconductivity*, 1991 (Plenum Press, New York, in press).
[31]C.T. Chen *et al.*, Phys. Rev. Lett. **68**, 2543 (1992).
[32]S. Kambe, H. Yasuoka, A. Hiyashi, and Y. Ueda, Phys. Rev. B **48**, 6593 (1993).
[33]P.C. Hammel, A.P. Reyes, S.W. Cheong, Z. Fisk, and J.E. Schirber Phys. Rev. Lett. **71**, 440 (1993).
[34]J.D. Perkins, J.M. Graybeal, M.A. Kastner, R.J. Birgenau, J.P. Falck, and M. Greven, Phys. Rev. Lett. **71**, 1621 (1993).
[35]J.C. Slater and G.F. Koster, Phys. Rev. **94**, 1498 (1954).
[36]These relations follow from the equation

$$t_{ij} = \frac{t_{pi} t_{pj}}{\epsilon_p - \epsilon_d}$$

and considering that $t_{px} = \sqrt{3}|t_{pz}|$ [see, for example, Walter A. Harrison, *Electronic Structure and the Properties of Solids* (Freeman, San Francisco, 1980)].
[37]W.L. McMillan, Phys. Rev. **167**, 331 (1968).
[38]W.H. Press, B.P. Flannery, S.A. Teukolsky, and W.T. Vetterling, *Numerical Recipes in Fortran* (Cambridge University Press, Cambridge, 1989), pp. 294–300.
[39]R. Micnas, J. Ranninger, and S. Robaszkiewicz, Rev. Mod. Phys. **62**, 113 (1990).
[40]S.R. White, D.J. Scalapino, R.L. Sugar, N.E. Bickers, and R.T. Scalettar, Phys. Rev. B **39**, 839 (1989); E. Dagotto, J. Riera, and A.P. Young, *ibid.* **42**, 2347 (1990).
[41]A. Bianconi, P. Castrucci, A. Fabriozi, M. Pompa, A.M. Flank, P. Lagarde, H. Katayama-Yoshida, and G. Calestani, in *Earlier and Recent Aspects of Superconductivity*, edited by J.G. Bednorz and K.A. Müller (Springer-Verlag, Berlin, 1990), p. 407.
[42]R. Joynt, Phys. Rev. B **41**, 4271 (1990).
[43]D.S. Harashima and T. Matsuura, J. Phys. Soc. Jpn. **59**, 24 (1990).
[44]J.F. Annett, N. Goldenfeld, and S.R. Renn, in *Physical Properties of High Temperature Superconductors,* edited by D.M. Ginsberg (World Scientific, Singapore, 1990), Vol. II, p. 571.